Accepted Manuscript

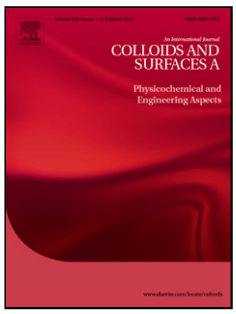

Title: On the Resolution of Constant Isosteric Heat of Propylene Adsorption on Graphite in the Sub-Monolayer Coverage Region

Author: Luisa Prasetyo Mus'ab Abdul Razak D.D. Do Toshihide Horikawa Kazuyuki Nakai D. Nicholson

PII: S0927-7757(16)30895-0
DOI: http://dx.doi.org/doi:10.1016/j.colsurfa.2016.10.040
Reference: COLSUA 21107

To appear in: *Colloids and Surfaces A: Physicochem. Eng. Aspects*

Received date: 29-8-2016
Revised date: 9-10-2016
Accepted date: 16-10-2016

Please cite this article as: Luisa Prasetyo, Mus'ab Abdul Razak, D.D.Do, Toshihide Horikawa, Kazuyuki Nakai, D.Nicholson, On the Resolution of Constant Isosteric Heat of Propylene Adsorption on Graphite in the Sub-Monolayer Coverage Region, Colloids and Surfaces A: Physicochemical and Engineering Aspects http://dx.doi.org/10.1016/j.colsurfa.2016.10.040

On the Resolution of Constant Isosteric Heat of Propylene Adsorption on Graphite in the Sub-Monolayer Coverage Region

by

Luisa Prasetyo[1], Mus'ab Abdul Razak[2], D. D. Do[1], Toshihide Horikawa[3], Kazuyuki Nakai[4] and D. Nicholson[1]

[1]School of Chemical Engineering
University of Queensland
St. Lucia, Qld 4072
Australia

[2] Department of Chemical and Environmental Engineering
Universiti Putra Malaysia
43400 Serdang
Malaysia

[3] Graduate School of Science and Technology
The University of Tokushima
2-1 Minamijosanjima, Tokushima 770-8506
Japan

[4] MicrotracBEL. Corp.
8-2-52 Nanko-Higashi, Suminoe-ku, Osaka 559-0031
Japan

* Author to whom all correspondence should be addressed. Email: d.d.do@uq.edu.au

TOC Graphic

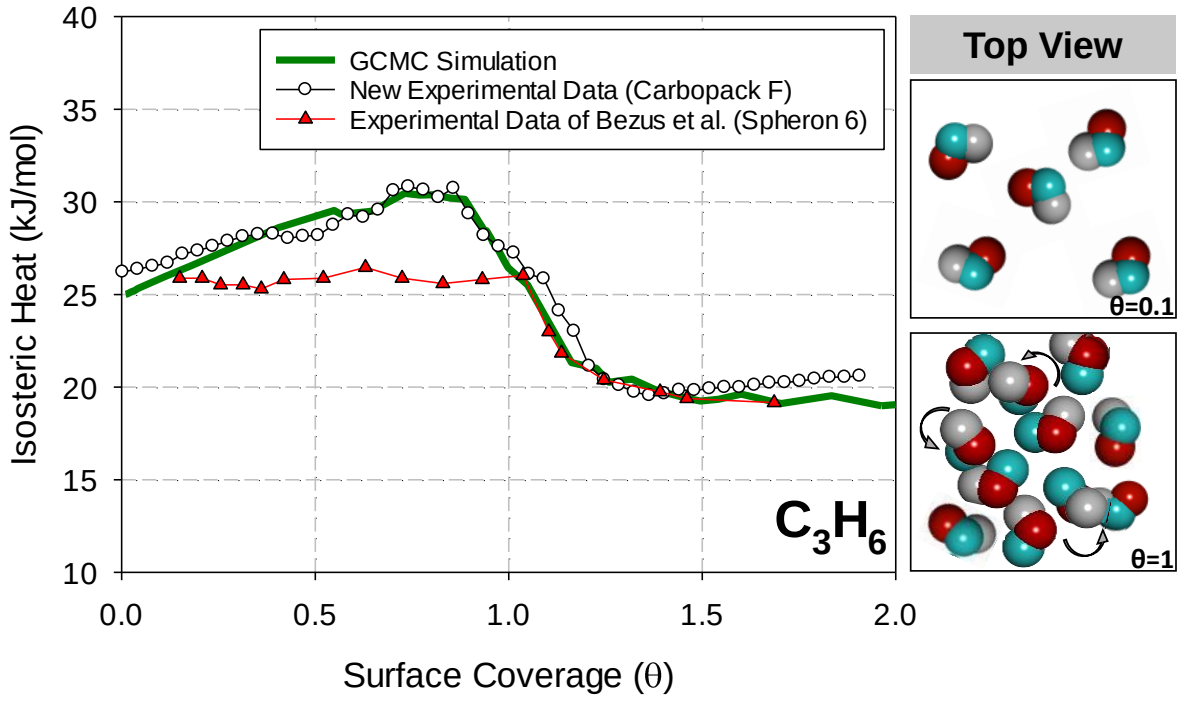

Highlights

- Resolution of isosteric heat versus loading for propylene adsorption on graphite
- Importance of the solid-fluid (SF) interaction with orientation of propylene
- Extensive simulation study of propylene adsorption with various potential models
- The dominance of adsorbate interactions over the SF interactions

Abstract

An early experimental study by Bezus, Dreving and Kiselev [1] on the adsorption of propylene on Spheron-6 carbon black (graphitized at ~3000C) reported a plot of constant isosteric heat versus loading in the sub-monolayer region. This contrasts with their report of a linear increase in isosteric heat for propane, a similar molecule to propylene. In this paper, we report extensive Grand Canonical Monte Carlo (*GCMC*) simulations and a high-resolution experimental study of propylene adsorption on Carbopack F, a highly graphitized thermal carbon black, over the same temperature range studied by Bezus *et al*. From this combined simulation and experimental study we conclude that propylene also shows a linear increase in the isosteric heat versus loading in the sub-monolayer region, indicating that the linear increase in the fluid-fluid interaction in this region more than compensates for the decrease in the solid-fluid interaction that results from the change in orientation of the adsorbate molecules. Our study contradicts the propylene results of Bezus *et al*., and careful

inspection of their isotherm in the sub-monolayer region shows that it does not follow Henry's law. This calls into question their argument that π-π interactions between propylene molecules are an explanation for the constant heat.

1. Introduction

An experimental study of propane and propylene adsorption on highly graphitized thermal carbon black (*GTCB*) Spheron 6 (3000^0) reported in 1961 by Bezus *et al*. [1], shows quite similar adsorption isotherms for these adsorbates, but interestingly the plots of isosteric heat versus loading for these two adsorbates are distinctly different in the sub-monolayer coverage region. The isosteric heat of propane shows a linear increase with loading (as typically observed for simple gases) while that of propylene is constant in the sub-monolayer region. These authors put forward the argument that the weaker adsorbate-adsorbate interaction of propylene, could be attributed to the lower polarizability of propylene due to $\pi - \pi$ interactions. This lacks credibility because the isotherms of propane and propylene are similar. In another study by Isirikyan and Kiselev [2] on adsorption of benzene on *GTCB*, a constant isosteric heat versus loading in the sub-monolayer region was also reported. This observation was explained, with the aid of a molecular simulation study [3], as being due to the balance between the increase in the fluid-fluid (*FF*) interaction, and the decrease in the solid-fluid (*SF*) interaction, brought about by the change in the orientation of some benzene molecules from their initial parallel orientation with the graphite surface to a 45 degree orientation with the surface. This then raises the question of whether this compensating balance might be applicable to propylene as well. It is the objective of this paper to re-examine this type of explanation for propylene adsorption and to test the argument for the role of π-π interactions put forwarded by Kiselev and co-workers.

Our initial premise is that the argument of Kiselev and co-workers is plausible because we have tested their experimental data for many sorbates against computer simulation and found perfect agreement (argon [4], nitrogen [5], methane [6], ethane [7], ethylene [7], carbon tetrachloride [8], carbon dioxide [9], benzene [3], n-butane, n-pentane and n-hexane [10] , methanol [11, 12], ethanol [12] and ammonia [13]). Therefore, the hypothesis is that the increase in isosteric heat from the increasing FF contribution, compensates exactly for the decrease in isosteric heat from the SF contribution, in the case of propylene adsorption. However, our preliminary simulation work on propylene adsorption on graphite has shown that the simulated isosteric heat versus loading does not support the observations of Kiselev

and co-workers. This has prompted us to embark on a combined study of experiment and molecular simulation in order to re-examine the isosteric heat versus loading for propylene and to establish the relative contributions from the fluid-fluid interaction and the solid-fluid interaction.

2. Experimental

2.1 Materials

A highly graphitized thermal carbon black, Carbopack F (supplied by Supelco, USA) was used as an adsorbent. This consists of polyhedral micro-particles with homogeneous graphene layers on the faces of the polyhedra. The *BET* surface area is 4.9 m^2/g and there are no detectable micropores or mesopores [14-16].

2.2 Measurement

Propylene adsorption at 230, 235 and 240K on Carbopack F was measured using a high-resolution volumetric adsorption apparatus with a cryostat (BELSORP-max, MicrotracBEL). The solid sample was degassed at 473K for 5 hours under vacuum at pressures less than 0.1 mPa to remove any physically adsorbed molecules prior to each measurement.

2.3 Isosteric heat of adsorption

The isosteric heat of adsorption (q_{st}) for each adsorbate was calculated by applying the Clausius-Clapeyron (*CC*) equation to the isotherm data:

$$q_{st} = \frac{RT_1T_2}{T_2 - T_1} \ln\left(\frac{P_2}{P_1}\right) \quad (1)$$

where R is the gas constant, T_1 and T_2 are the adsorption temperatures and P_1 and P_2 are the respective absolute pressures at a given loading.

3. Theory

3.1 GCMC simulations

In the Grand Canonical Monte Carlo (*GCMC*) simulations we used 100,000 cycles for both equilibration and sampling stages. Each cycle, consisted of 1000 attempted displacement, insertion and deletion moves, chosen with equal probability. In the equilibration stage, the maximum displacement step length was initially set as 2nm, and was adjusted at the end of each cycle to give an acceptance ratio of 20%. The lengths of the simulation box in the *x* and *y* directions were 15 times the collision diameter of the methyl group (modelled as a united atom of diameter 0.361 nm in propylene) and the dimension in the *z*-direction was 5 nm. The

graphite surface was infinite in the *x* and *y* directions (modelled with periodic boundary conditions), and the atom centres in the uppermost graphene layer of the *GTCB* were positioned at $z = 0$ and a hard wall was positioned at $z = 5$nm.

3.2 Potential Energies

Among the many potential models available in the literature for propylene, for example: *TraPPE* [17], *AUA4* [18], *OPLS-UA* [19], *Vrabec* [20], *NERD* [21], *SET* [22], we chose the *AUA4* model as it gives the best description of the vapour-liquid equilibrium for propylene; its molecular parameters are given in Table 1. The interaction potential energies were assumed to be pairwise additive and the adsorbate-adsorbate interaction energy was described by a 12−6 Lennard-Jones (LJ) equation. The graphite surface was modelled as a structure-less solid, and its interaction energy with an LJ site of an adsorbate molecule was calculated from the Steele 10-4-3 equation [23]. The surface density of carbon in a graphene layer is 38.2nm^{-2}, its molecular parameters are σ_{ss} = 0.34 nm and ε_{ss} / k_B = 28K, and the interlayer spacing between two adjacent graphene layers is 0.3354 nm. The cross molecular parameters were calculated by the Lorentz-Berthelot mixing rule, and the cross well depth of interaction was adjusted with a binary interaction parameter, $\varepsilon'_{sf} = (1-k_{sf})\varepsilon_{sf}$, so that the simulated Henry constant agrees with the experimental Henry constant.

3.3 Thermodynamic Properties

Surface Excess

The surface excess concentration is defined as:

$$\Gamma_{ex} = \frac{N_{ex}}{L_x L_y} = \frac{\langle N \rangle - V_{acc}\rho_G}{L_x L_y} \tag{2}$$

where N_{ex} is the excess amount adsorbed, $\langle N \rangle$ is the ensemble average of the number of particles in the simulation box, ρ_G is the bulk gas density, V_{acc} is the accessible volume, L_x and L_y are the box dimensions in the *x*- and *y*-directions, respectively.

Isosteric Heat

The isosteric heat was calculated from the fluctuation theory [24]:

$$q_{st} = \frac{\langle U \rangle \langle N \rangle - \langle UN \rangle}{\langle N^2 \rangle - \langle N \rangle^2} + R_g T$$

where *U* is the sum of the potential energy due to fluid-fluid interactions (U_{FF}) and that due to solid-fluid interaction (U_{SF}). The solid-fluid energy can be divided into contributions from the three LJ sites in propylene molecule: $U_{SF} = U_{SF}^{LJSite1} + U_{SF}^{LJSite2} + U_{SF}^{LJSite3}$.

Local Density Distribution

To study the variation in density from the surface, the local density of the centre of geometry (which is defined as $\underline{r}_{COG} = \left(\sum_{j=1}^{M} \underline{r}_j \right) / M$, where *M* is the number of sites in a molecule) of the adsorbate is defined as:

$$\rho(z) = \frac{\langle \Delta N_{z+\Delta z} \rangle}{L_x L_y \Delta z} \tag{3}$$

where $<\Delta N_{z+\Delta z}>$ is the ensemble average of the number of molecules whose centre of geometry is located in the region bound between *z* and $z+\Delta z$. The local density of a specific LJ site was also calculated from the same equation with $\Delta N_{z+\Delta z}$ defined as the number of a given LJ site.

Theoretical Henry Constant and Isosteric Heat at Zero Loading

To study the interaction between an adsorbate and the basal plane, the isosteric heat at zero loading $q_{st}^{(0)}$ and the Henry constant, contributed solely from the basal plane (K_B) can be calculated as given by Do *et al*. [25], using the Monte Carlo integration:

$$K_B = \frac{1}{A}\left\{ \int_{\Omega} \exp\left[-\beta\varphi(r,\omega)\right] dr d\omega - \int_{\Omega} H\left[-\varphi(r,\omega)\right] dr d\omega \right\} \tag{4}$$

$$q_{st}^{(0)} = k_B T - k_B T \frac{\int\int_{\omega\,\Omega} \left[\beta\varphi(r,\omega)\right] \exp\left[-\beta\varphi(r,\omega)\right] dr d\omega}{\int\int_{\omega\,\Omega} \exp\left[-\beta\varphi(r,\omega)\right] dr d\omega - V_{acc}} \tag{5}$$

where Ω is the domain accessible to adsorbate, *A* is the surface area of the solid, $\beta = (k_B T)^{-1}$, φ is the potential energy of interaction between an adsorbate molecule at the position ***r*** and an orientation ω and the graphite surface and H is the Heaviside step function.

4. Results and Discussion

4.1 Theoretical Henry Constant and Isosteric Heat at Zero Loading of Propylene

The Henry constant calculated from eq. (4) for propylene adsorption on graphite is plotted in Figure 1a as a function of temperature. To assess the affinity of propylene for the graphite surface, we also show in the same figure the Henry constant of a number of adsorbates commonly used in the characterization of porous solids. The affinity of propylene is very similar to that of propane, and both of them are one or more orders of magnitude greater than methanol, ammonia, argon or water. Propylene and propane both have a higher isosteric heat at zero loading (Figure 1b) because each has 3 strong interaction centres which can lie close to the surface and which generate a greater potential energy well depth than the other adsorbates. To ensure agreement between the theory and experimental data, the well depth of propylene-graphite calculated from the Lorentz-Berthelot rule is multiplied by a factor of 1.02, and Table 2 shows this agreement with the isosteric heat at zero loading.

4.2 Adsorption Isotherm

Figure 2 shows the adsorption isotherm data for propylene on graphitized Spheron 6 (3000^0) at 228K from Bezus *et al.* [1] and our experimental data for Carbopack on linear scales. At first sight these data seem to be in good agreement with each other, and also with the *GCMC* simulation results. However, when we present these experimental data and the simulation results on a logarithmic scale, to highlight better the sub-monolayer coverage region, we observe a distinct difference between our data and the data of Kiselev. Their results fail to obey Henry's law and this behaviour is a clear signature that the surface of their Spheron 6 (3000^0) may not have been homogeneous. This would lead to a gradual decrease in the solid-fluid interaction as coverage increased, in addition to the orientational change of propylene molecule. Furthermore, our data obey Henry's law and agree with the *GCMC* simulation results perfectly in the sub-monolayer coverage region.

4.3 Isosteric Heat

Figure 3 shows the *GCMC* simulated isosteric heat versus loading and the experimental data from our work and also from Bezus *et al*. Our experimental data and the *GCMC* simulation results agree well with each other, in the same manner as we have observed for the analysis of the adsorption isotherms in Section 4.2. Our experimental heat increases linearly with loading in the sub-monolayer coverage region (up to θ=0.8, where θ is the fractional monolayer coverage concentration of 5.3μmol/m^2), in agreement with not only the simulation

results using the AUA4 potential model, but also with other potential models (Appendix-Figure A1) for propylene available in the literature. This further corroborates our argument that the constant isosteric heat profile of Bezus *et al*. for loadings below the monolayer coverage is in error.

Decomposition of Isosteric Heat Profile

To understand the microscopic origin of the linear increase in isosteric heat in the sub monolayer region, we decomposed the simulated isosteric heat into contributions from solid-fluid (*SF*) and fluid-fluid (*FF*) interactions in Figure 3. There is an initial decrease in the *SF* contribution, a trend that is not commonly observed for simple gases (i.e. Ar [30], Kr [31]), suggesting that there is a change in the molecular orientation of propylene as molecules begin to fill the monolayer. To shed further light on this, we decomposed the *SF* contribution into contributions from the three LJ-sites of propylene as shown in Figure 4. The CH group makes the least contribution as it has the smallest ε/k_B value (see Table 1) compared to the other two sites, CH_3 and CH_2. All these sites have the same decrease with loading in the sub-monolayer coverage, indicating that there is no preference which LJ site is pointing away from the surface.

Even though there is a decrease in the *SF* contribution to the isosteric heat, due to the change in orientation of some propylene molecules (see below), the full heat curve shows that the increase in the *FF* contribution does not entirely compensate for this, and that the overall trend is a linear increase in the isosteric heat in the sub monolayer region. The gradual increase in the *FF* interactions conflicts with the arguments of Kiselev and co-workers that repulsive $\pi - \pi$ interactions between propylene molecules weaken the *FF* interactions, and therefore decrease the *FF* contribution to the isosteric heat.

Local Density Distribution Analysis

To better understand the preferential orientation of propylene at various loadings, we present in Figure 5 the local density distribution of the centre of geometry (*COG*) of propylene for various loadings. The first and second layers are located about 0.35nm and 0.75nm, respectively, from the surface. As the loading is increased, a shoulder appears in the first peak, indicating a change in the orientation of some molecules because the increase in the number of possible configurations with the same energy facilitates a shift of the *COGs* away from the surface (an entropic effect).

Figure 6 shows the local density distribution for each of the three LJ sites, and the snapshots of the first layer of propylene adsorbed on graphite at selected loadings are shown in Fig. 7.

From Figures 6 and 7, a number of points can be highlighted:

a) At low loading (θ = 0.1 in Figure 6a), the majority of propylene molecules in the first layer adopt a parallel orientation (a single peak is observed for all LJ sites, CH_3, CH_2 and CH; i.e. they are in contact with the graphite surface to maximize the *SF* interaction). Interestingly, there is a very small, but noticeable shoulder associated with the CH site. This shoulder represents a small population of propylene molecules that have the CH site pointing away from the surface (see the circled molecule in Figure 7a). Similar behaviour is observed at loadings with up to 40% of the surface covered with molecules (θ = 0.4; see Figures 6b and 7b).

b) At the monolayer coverage (θ = 1), we observe both molecules with CH pointing away from the surface, but also molecules having either CH_2 or CH_3 or both (Figure 6c) pointing away from the surface; however, most of the propylene molecules remain parallel to the surface. This orientational change of some propylene molecules when the monolayer is being filled maximizes the number of molecules that can be packed into the first layer by maximizing the *FF* interactions which over-compensate for the reduction in the *SF* interactions (because of the orientational change), leading to an overall reduction of the Gibbs free energy.

c) When loading reaches twice the monolayer coverage (θ = 2.0), the first layer acts as a quasi-surface for propylene molecules adsorbing in the second layer as seen in Figure 8. The local density profile of all sites (Figure 6d) indicates that molecules in the first layer interact not only with the graphite surface but also with molecules in the higher layers and as a result their orientations are continually changing as the second layer is being built up. The region marked with a circle in the snapshot in Figure 7d highlights the randomisation of propylene orientations in the first layer in order to maximise their *FF* interactions with their neighbours in both the first and second layers.

A general deduction is that molecular orientation plays an important role in determining the way that the isosteric heat varies with loading. As the loading is increased, molecules continually change their orientation, causing a shift in the position of the *COG* as seen in Figure 5, which shows that when θ is increased from 1.7 to 2, the shoulder in the first layer distribution increases in intensity at the expense of the main peak in the first layer distribution. This is consistent with molecules in the first layer changing from orientations parallel to the surface to non-parallel ones. We also note that as the second layer is filled with propylene molecules, there is a transfer of molecules from the second layer to the first layer. To substantiate this we decomposed the adsorption isotherm into contributions from the first layer and from the second layer as shown in Figure 9, which shows that there is compression of the first layer even after θ = 1 has been reached.

5. Conclusion

The adsorption mechanism and isosteric heat of propylene on Carbopack F have been re-investigated using high-resolution experiment and *GCMC* simulation. Our findings have shown that the isosteric heat of propylene has an increasing trend with loading in the sub-monolayer coverage region, contrary to the constant isosteric heat profile originally reported by Bezus *et al*. Our new results find no evidence for a repulsive π–π interaction as suggested by these authors. We do note that there is a reduction of adsorbate-adsorbent interaction in the sub-monolayer region, which can be attributed to a change in propylene orientation, however, this is not sufficient to cancel the heat contributed by the adsorbate-adsorbate interaction.

Acknowledgement: This project is funded by the Australian Research Council (DP160103540)

References

1. Bezus, A., V. Dreving, and A. Kiselev, *Isotherms and heats of adsorption of propane and propylene on graphitized carbon black - energy of adsorption forces.* Kolloidnyi Zhurnal, 1961. **23**(4): p. 389.
2. Isirikyan, A. and A. Kiselev, *The absolute adsorption isotherms of vapors of nitrogen, benzene and n-hexane, and the heats of adsorption of benzene and n-hexane on graphitized carbon*

blacks. I. Graphitized thermal blacks. The Journal of Physical Chemistry, 1961. **65**(4): p. 601-607.

3. Do, D. and H. Do, *Adsorption of benzene on graphitized thermal carbon black: Reduction of the quadrupole moment in the adsorbed phase.* Langmuir, 2006. **22**(3): p. 1121-1128.
4. Wongkoblap, A., D.D. Do, and D. Nicholson, *Explanation of the unusual peak of calorimetric heat in the adsorption of nitrogen, argon and methane on graphitized thermal carbon black.* Physical Chemistry Chemical Physics, 2008. **10**(8): p. 1106-1113.
5. Do, D. and H. Do, *Adsorption of quadrupolar, diatomic nitrogen onto graphitized thermal carbon black and in slit-shaped carbon pores. Effects of surface mediation.* Adsorption Science & Technology, 2005. **23**(4): p. 267-288.
6. Do, D. and H. Do, *Evaluation of 1-site and 5-site models of methane on its adsorption on graphite and in graphitic slit pores.* The Journal of Physical Chemistry B, 2005. **109**(41): p. 19288-19295.
7. Do, D. and H. Do, *Effects of potential models on the adsorption of ethane and ethylene on graphitized thermal carbon black. Study of two-dimensional critical temperature and isosteric heat versus loading.* Langmuir, 2004. **20**(25): p. 10889-10899.
8. Do, D. and H. Do, *Adsorption of carbon tetrachloride on graphitized thermal carbon black and in slit graphitic pores: five-site versus one-site potential models.* The Journal of Physical Chemistry B, 2006. **110**(19): p. 9520-9528.
9. Do, D. and H. Do, *Effects of potential models on the adsorption of carbon dioxide on graphitized thermal carbon black: GCMC computer simulations.* Colloids and Surfaces A: Physicochemical and Engineering Aspects, 2006. **277**(1): p. 239-248.
10. Do, D. and H. Do, *Adsorption of flexible n-alkane on graphitized thermal carbon black: analysis of adsorption isotherm by means of GCMC simulation.* Chemical engineering science, 2005. **60**(7): p. 1977-1986.
11. Nguyen, V.T., D. Do, D. Nicholson, and J. Jagiello, *Effects of temperature on adsorption of methanol on graphitized thermal carbon black: a computer simulation and experimental study.* The Journal of Physical Chemistry C, 2011. **115**(32): p. 16142-16149.
12. Birkett, G. and D. Do, *Simulation study of methanol and ethanol adsorption on graphitized carbon black.* Molecular Simulation, 2006. **32**(10-11): p. 887-899.
13. Birkett, G. and D. Do, *Simulation study of ammonia adsorption on graphitized carbon black.* Molecular Simulation, 2006. **32**(7): p. 523-537.
14. Horikawa, T., M. Takenouchi, D.D. Do, K.-I. Sotowa, J.R. Alcántara-Avila, and D. Nicholson, *Adsorption of water and methanol on highly graphitized thermal carbon black and activated carbon fibre.* Australian Journal of Chemistry, 2015. **68**(9): p. 1336-1341.
15. Horikawa, T., T. Muguruma, D. Do, K.-I. Sotowa, and J.R. Alcántara-Avila, *Scanning curves of water adsorption on graphitized thermal carbon black and ordered mesoporous carbon.* Carbon, 2015. **95**: p. 137-143.
16. Horikawa, T., Y. Zeng, D. Do, K.-I. Sotowa, and J.R.A. Avila, *On the isosteric heat of adsorption of non-polar and polar fluids on highly graphitized carbon black.* Journal of colloid and interface science, 2015. **439**: p. 1-6.
17. Wick, C.D., M.G. Martin, and J.I. Siepmann, *Transferable potentials for phase equilibria. 4. United-atom description of linear and branched alkenes and alkylbenzenes.* The Journal of Physical Chemistry B, 2000. **104**(33): p. 8008-8016.
18. Bourasseau, E., M. Haboudou, A. Boutin, A.H. Fuchs, and P. Ungerer, *New optimization method for intermolecular potentials: Optimization of a new anisotropic united atoms potential for olefins: Prediction of equilibrium properties.* The Journal of chemical physics, 2003. **118**(7): p. 3020-3034.
19. Jorgensen, W.L., J.D. Madura, and C.J. Swenson, *Optimized intermolecular potential functions for liquid hydrocarbons.* Journal of the American Chemical Society, 1984. **106**(22): p. 6638-6646.

20. Vrabec, J., J. Stoll, and H. Hasse, *A set of molecular models for symmetric quadrupolar fluids.* The Journal of Physical Chemistry B, 2001. **105**(48): p. 12126-12133.
21. Nath, S.K., B.J. Banaszak, and J.J. de Pablo, *A new united atom force field for α-olefins.* The Journal of Chemical Physics, 2001. **114**(8): p. 3612-3616.
22. Spyriouni, T., I.G. Economou, and D.N. Theodorou, *Molecular Simulation of α-Olefins Using a New United-Atom Potential Model: Vapor-Liquid Equilibria of Pure Compounds and Mixtures.* Journal of the American Chemical Society, 1999. **121**(14): p. 3407-3413.
23. Steele, W.A., *The physical interaction of gases with crystalline solids: I. Gas-solid energies and properties of isolated adsorbed atoms.* Surface Science, 1973. **36**(1): p. 317-352.
24. Nicholson, D. and G. Parsonage, *Computer simulation and the statistical mechanics of adsorption*. 1982, London: Academic Press.
25. Do, D., D. Nicholson, and H. Do, *On the Henry constant and isosteric heat at zero loading in gas phase adsorption.* Journal of colloid and interface science, 2008. **324**(1): p. 15-24.
26. Chen, B., J.J. Potoff, and J.I. Siepmann, *Monte Carlo calculations for alcohols and their mixtures with alkanes. Transferable potentials for phase equilibria. 5. United-atom description of primary, secondary, and tertiary alcohols.* The Journal of Physical Chemistry B, 2001. **105**(15): p. 3093-3104.
27. Kristof, T., J. Vorholz, J. Liszi, B. Rumpf, and G. Maurer, *A simple effective pair potential for the molecular simulation of the thermodynamic properties of ammonia.* Molecular Physics, 1999. **97**(10): p. 1129-1137.
28. Maitland, G.C., M. Rigby, E.B. Smith, and W.A. Wakeham, *Intermolecular Forces. Their Origin and Determination*. The international Series of Monographs on Chemestry. 1987, Oxford: Oxford Science Publications. xiv. 616.
29. Berendsen, H., J. Grigera, and T. Straatsma, *The missing term in effective pair potentials.* Journal of Physical Chemistry, 1987. **91**(24): p. 6269-6271.
30. Razak, M.a.A., V.T. Nguyen, L. Herrera, D. Do, and D. Nicholson, *Microscopic analysis of adsorption in slit-like pores: layer fluctuations of particle number, layer isosteric heat and histogram of particle number.* Molecular Simulation, 2011. **37**(12): p. 1031-1043.
31. Prasetyo, L., T. Horikawa, P. Phadungbut, S.J. Tan, D. Do, and D. Nicholson, *A GCMC simulation and experimental study of krypton adsorption/desorption hysteresis on a graphite surface.* Journal of Colloid and Interface Science, 2016. **478**: p. 402-412.

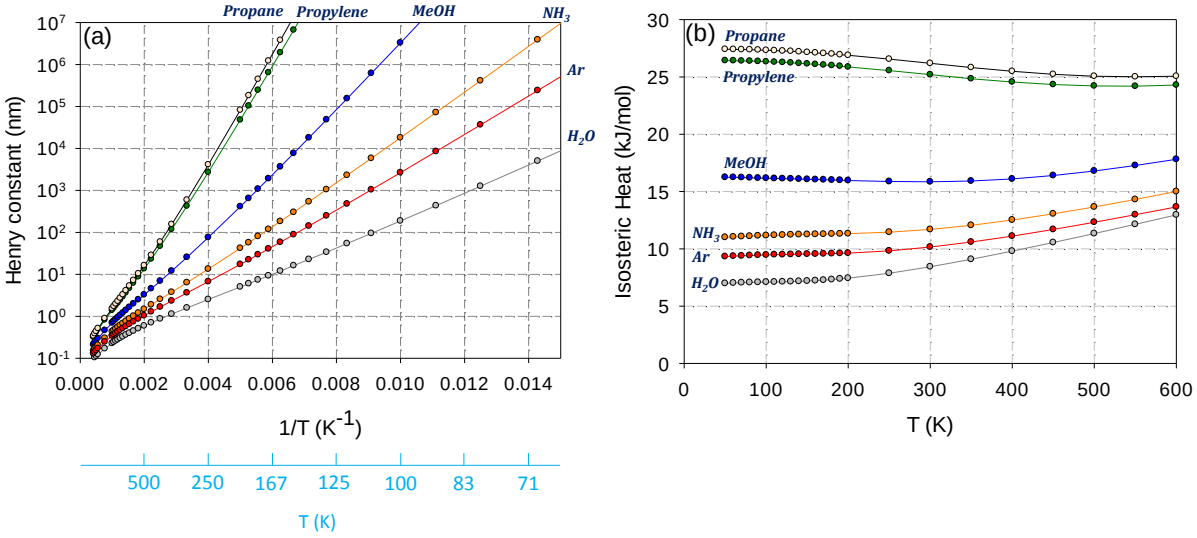

Figure 1-(a) Theoretical Henry constants K_B of various molecules on graphite(propane [18], propylene [18], methanol[26], ammonia [27], argon [28] and water [29]);(b) Isosteric heat at zero loading calculated using Monte Carlo integration technique. Note: no k_{sf} adjustment was used in these calculations.

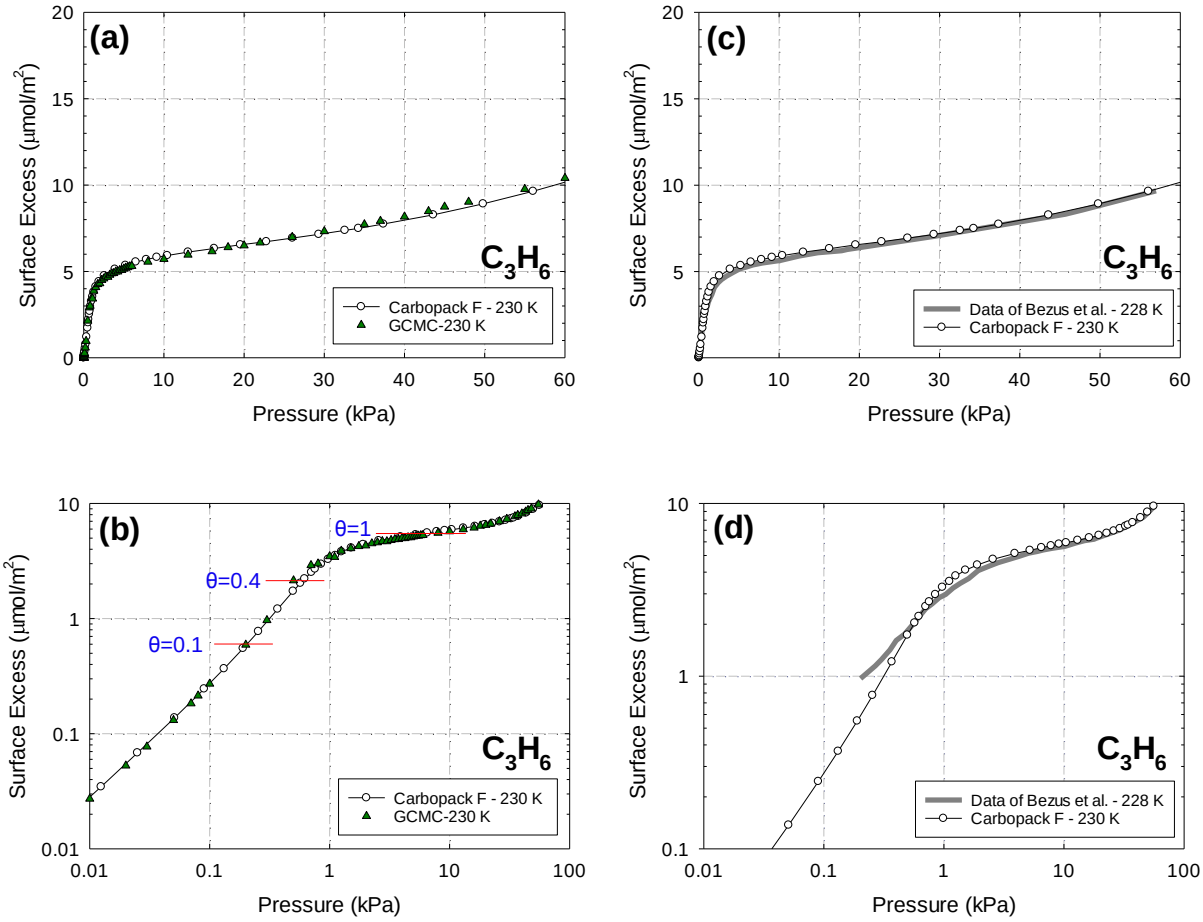

Figure 2-Experimental isotherm of propylene adsorption on Carbopack F at 230 K and GCMC simulated adsorption isotherm of propylene using the AUA4 model at 230 K (k_{sf}= - 0.02) :(a) linear scale, (b) log-log scale. Experimental isotherm of propylene adsorption on Carbopack F at 230 K and the adsorption isotherm of Bezus *et al*. at 228 K: (c) linear scale, (b) log-log scale.

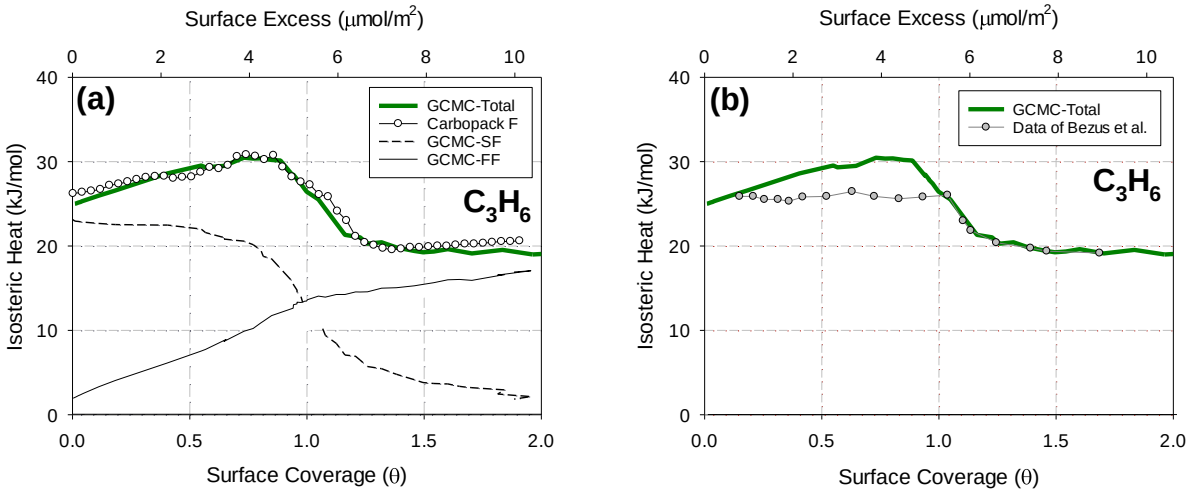

Figure 3- (a) GCMC simulated adsorption isosteric heats of propylene using the AUA4 model at 230 K (k_{sf} = -0.02), decomposed into heat contributed by solid-fluid and fluid-fluid interactions; experimental isosteric heat versus loading for propylene adsorption on Carbopack F, calculated from three isotherms at 230 K, 235 K and 240 K (this work). (b) Experimental isosteric heat versus loading from Bezus et al., calculated from three isotherms at 218 K, 228 K and 238 K.

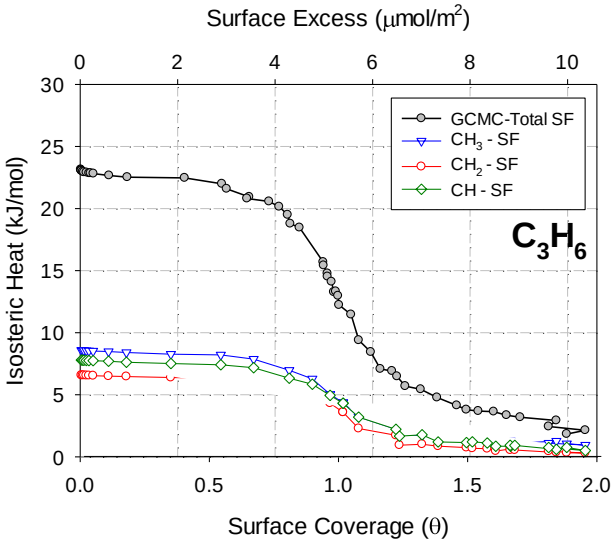

Figure 4- *GCMC* simulated *SF* isosteric heat profile of propylene using the AUA4 model at 230 K (k_{sf} = -0.02), decomposed into each united atom (CH_3-CH-CH_2) contributions.

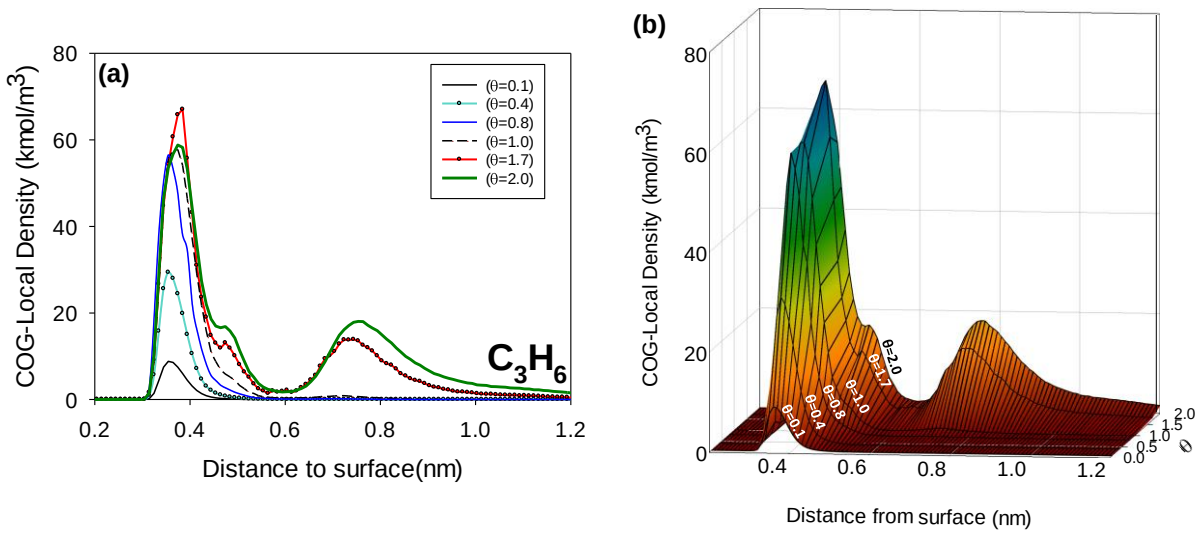

Figure 5- Local density distribution (based on the centre of geometry of propylene) as a function of distance to the graphite surface for propylene at 230K at various loadings (θ is the number of monolayers adsorbed). (a): 2D-graph, (b): 3D-graph.

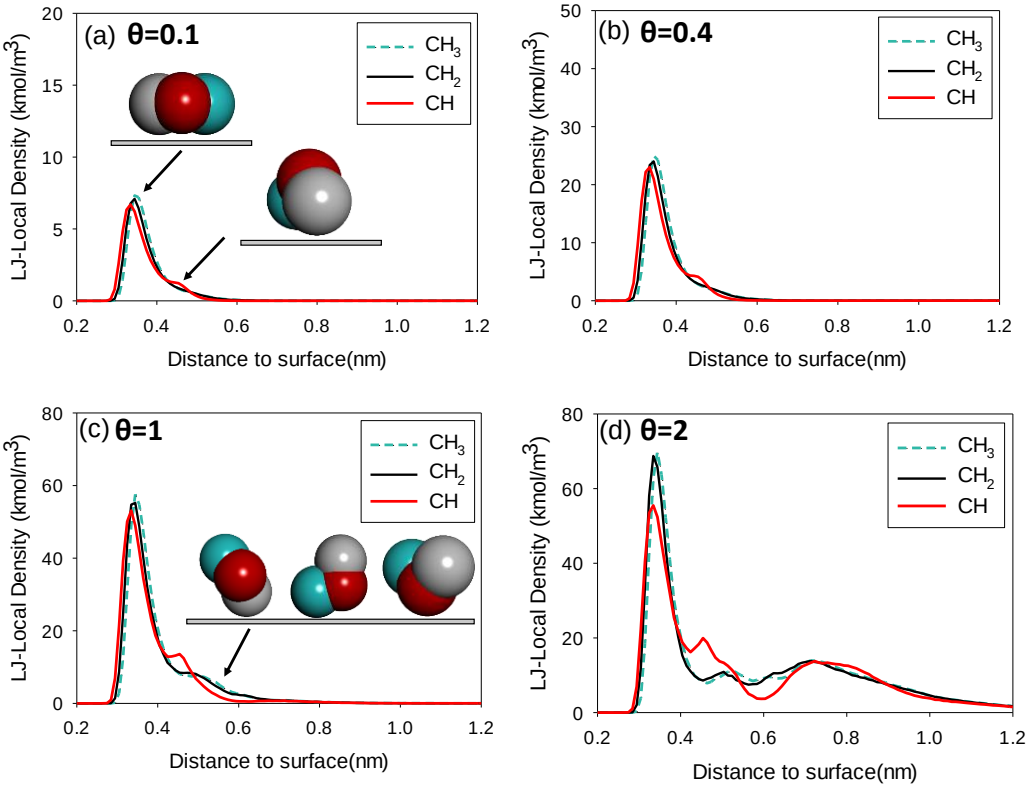

Figure 6- LJ local density distribution of propylene adsorption on graphite obtained with *GCMC* simulation at 230 K for loadings (a) θ = 0.1, (b) θ = 0.4, (c) θ = 1, (d) θ = 2. Red, blue and grey atoms are CH, CH_3 and CH_2, respectively.

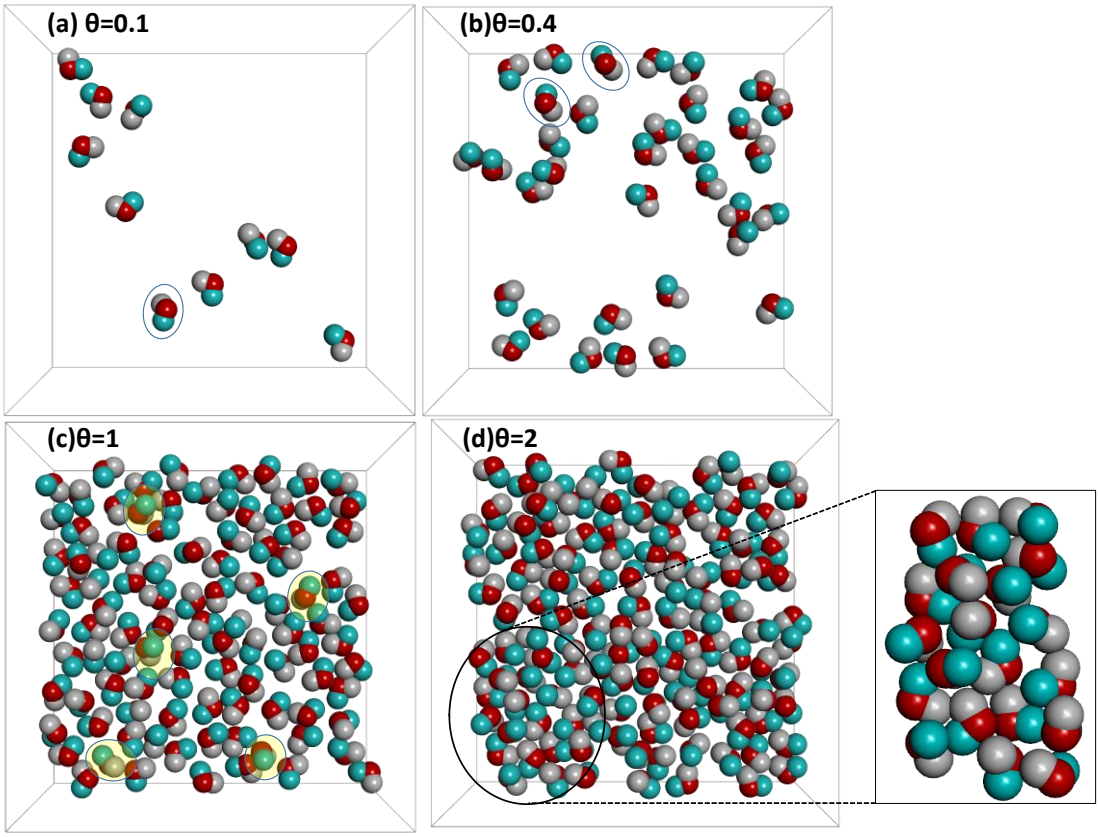

Figure 7-Top view snapshot of propylene adsorption (first layer only) on graphite obtained with GCMC simulation at 230 K (k_{sf} = -0.02) for different loadings (a) θ=0.1, (b) θ =0.4, (c) θ=1, (d) θ =2.

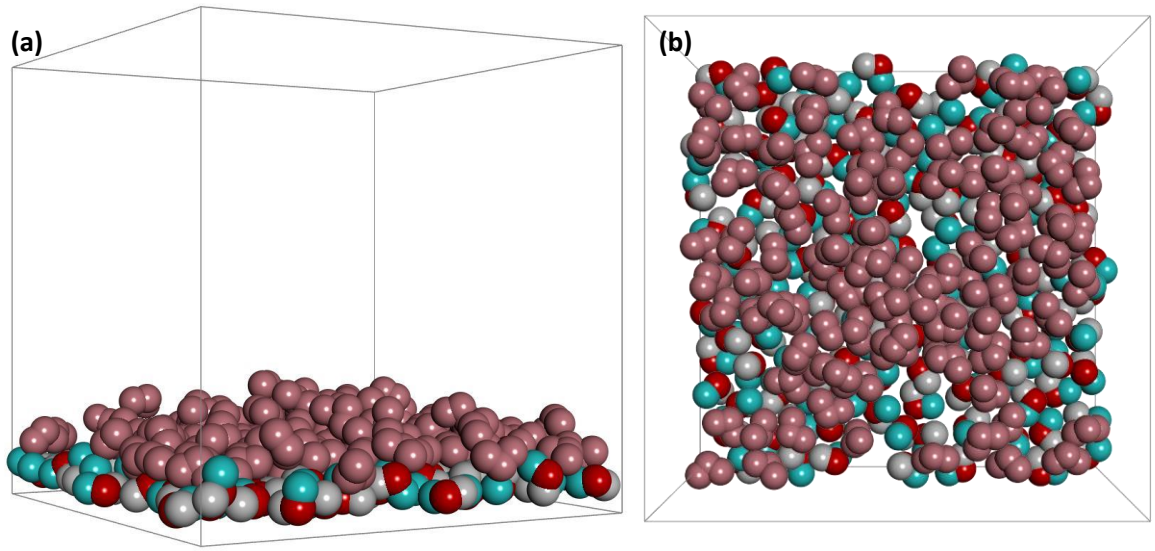

Figure 8- Snapshot of propylene adsorbed on graphite from GCMC simulation at 230 K (k_{sf} = -0.02), at θ=2: (a) simulation box, (b) top view of all molecules. Molecules coloured in purple represent propylene molecules adsorbed in the second layer.

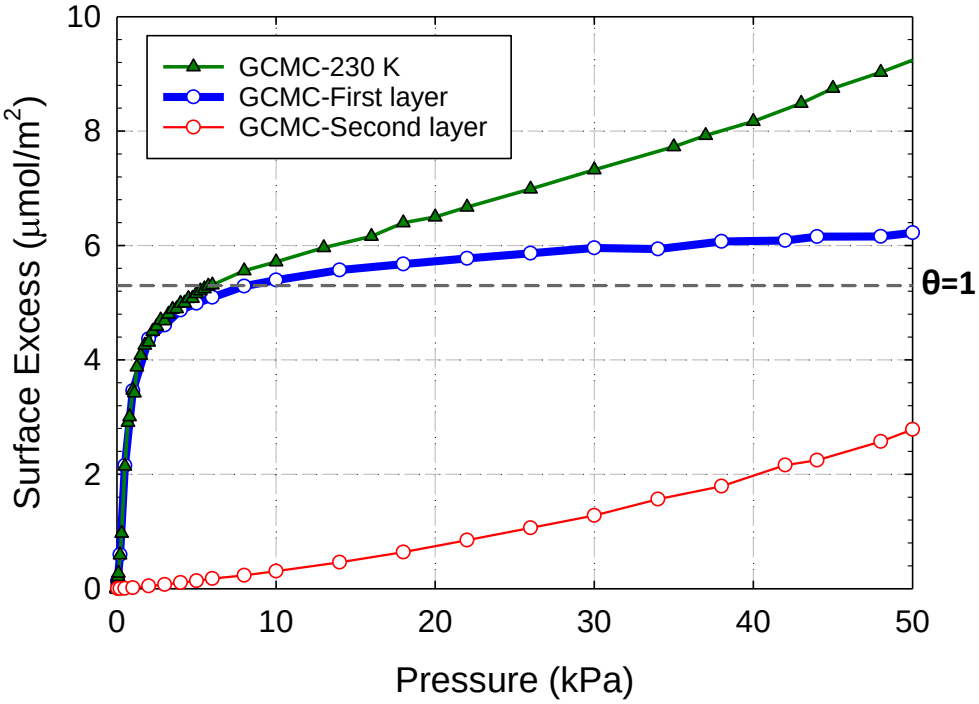

Figure 9- GCMC simulated adsorption isotherm of propylene using the AUA4 model at 230K (ksf= - 0.02): showing contributions to the total isotherm from first and second layers. The size of the bin in the z- direction is 0.6nm. The dashed line represents monolayer coverage for propylene adsorption at 230K.

GCMC Isosteric Heat Profile and Adsorption Isotherm of Propylene Adsorption on Graphite at 230K with Various Potential Models

(a)

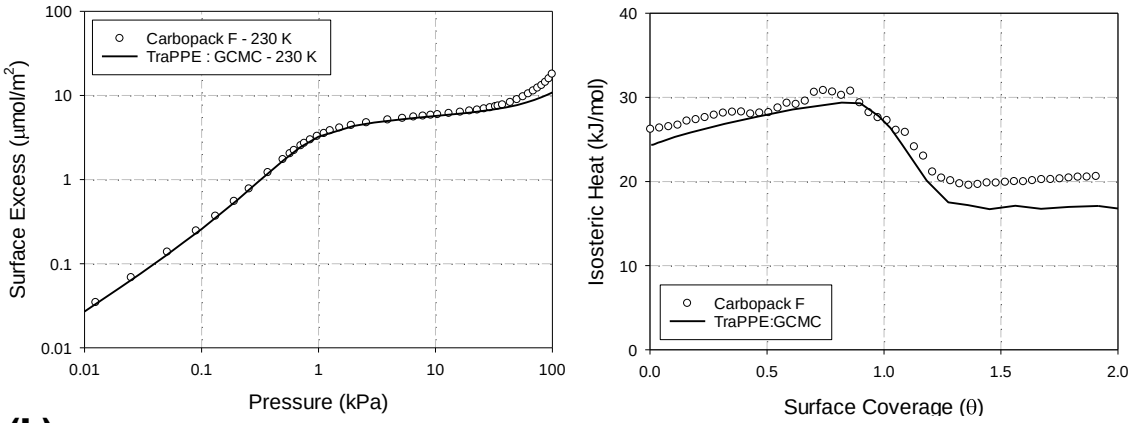

(b)

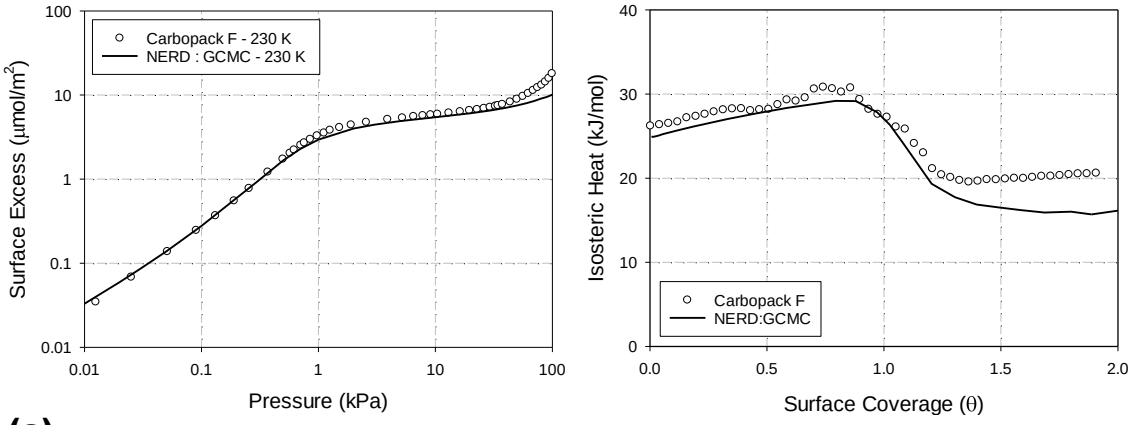

(c)

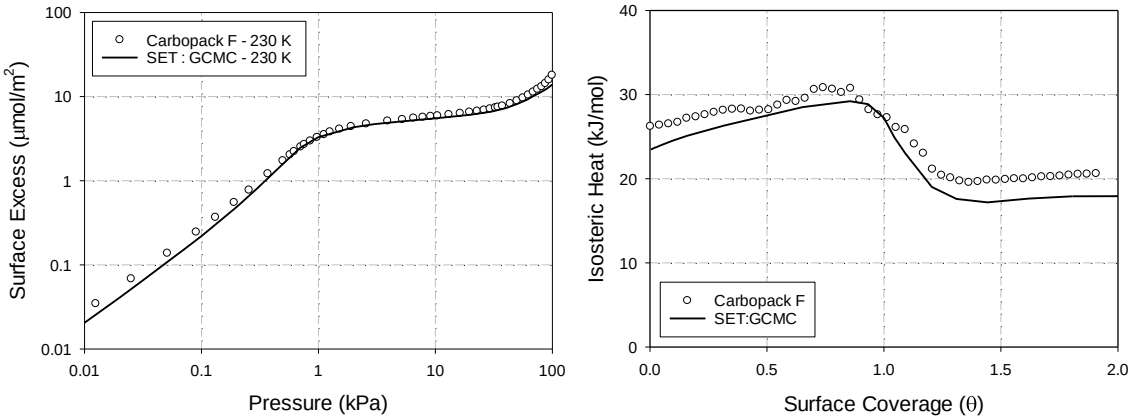

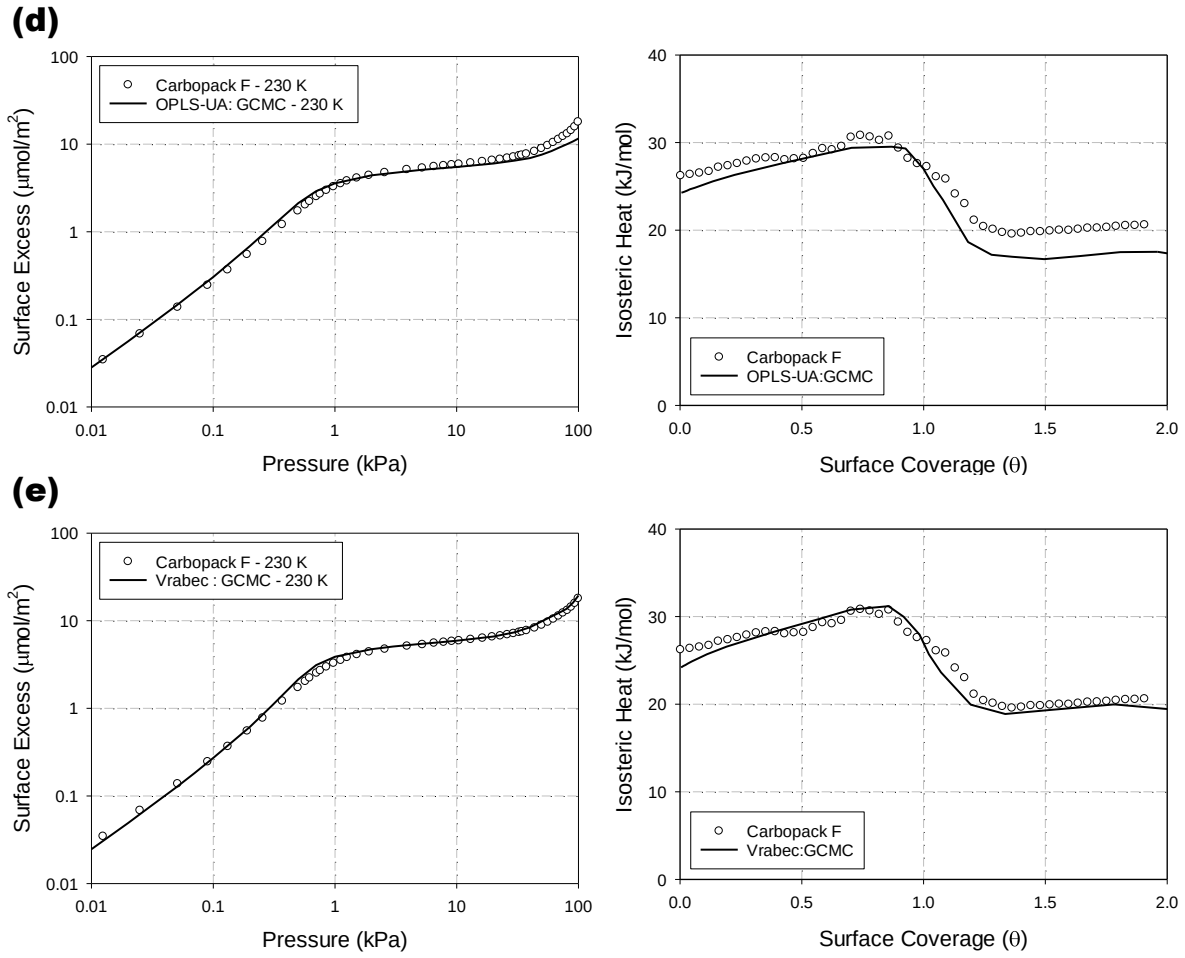

Figure A1 –Adsorption isotherms and isosteric heat profiles of propylene on graphitized thermal carbon black at 230 K. Empty symbols, experimental data of Carbopack F. Solid line, GCMC simulation results (with various k_{sf}) of several propylene potential models: (a) TraPPE(k_{sf}: -0.1), (b) NERD (k_{sf}: -0.12), (c)SET(k_{sf}: 0),(d)OPLS-UA (k_{sf}: -0.05),(e)Vrabec (k_{sf}: -0.06). The lengths of the simulation box in the x and y directions were 15 times, and that in z direction was 20 times, the collision diameter of the methyl group (of propylene). 50,000 cycles were used for both the equilibration and the sampling stage. Each cycle, consisted of 1000 attempted displacement, insertion and deletion moves, chosen with equal probability. The graphite surface was infinite in the x and y directions (modelled with periodic boundary conditions), and a hard wall was positioned at one boundary in the z-direction. The parameters for various propylene potential models are summarised in Table A1.

Table 1-Potential Parameters for Propylene (AUA4 model [18])

Model	Group	σ_{ff} (nm)	ε / k_B (K)	l_{C-C} (nm)	$l_{C=C}$ (nm)	θ_{C-C-C} (°)	δ^a (nm)
AUA-4	CH_3	0.361	120.1	0.1535	0.1331	124.0	0.0216
[18]	CH	0.332	90.6				0.0414
	CH_2	0.348	111.1				0.0295

*δ^a is the carbon to force field distance

Table 2- Isosteric heat at zero loading of propylene using the AUA4 model obtained by Monte Carlo integration (with k_{sf}= -0.02) compared with the new experimental data for the Carbopack F adsorbent.

Molecule	T(K)	$q_{st}^{(0)}$ (kJ/mol)	
		Monte Carlo Integration	Carbopack F
Propylene	230	26.23	26.2
	235	26.19	
	240	26.16	

6. Appendix

Parameters for Various Models of Propylene:

Table A1- Parameters for Various Potential Models of Propylene

Model	Group	σ_{ff} (nm)	ε / k_B (K)	$l_{C\text{-}C}$ (nm)	$l_{C=C}$ (nm)	$\theta_{C\text{-}C\text{-}C}$ (°)	δ^a (nm)	Q^{2*} (-)
AUA-4	CH_3	0.361	120.1				0.0216	
[18]	CH	0.332	90.6	0.1535	0.1331	124.0	0.0414	
	CH_2	0.348	111.1				0.0295	
TraPPE	CH_3	0.375	98					
[17]	CH	0.373	47	0.154	0.133	119.7		
	CH_2	0.3675	85					
NERD	CH_3	0.385	100					
[21]	CH	0.377	46	0.154	0.134	124.0		
	CH_2	0.372	92.5					
SET	CH_3	0.392	47.66					
[22]	CH	0.392	81.69	0.153	0.133	124.0		
	CH_2	0.391	89.93					
OPLS-UA	CH_3	0.391	88.1					
[19]	CH	0.380	57.9	0.150	0.134	124.0		
	CH_2	0.385	70.5					
Vrabec		0.38169	150.78	0.25014				2.0912
[20]								

*δ^a is the carbon to force field distance

*The Vrabec model is a 2CLJQ (two-center LJ plus point quadrupole) pair potential.